(Received 29 October 2024, Accepted 21 January 2025, Scheduled 3 February 2025)

Efficient Technique for HTS Coupled Resonator Filters Design Using an Enhanced FDTD Algorithm

Mohamed K. Laoufi[1], Slimane Mekaoui[1], Mohamed L. Tounsi[2,*], and Mustapha C. E. Yagoub[3]

[1] *LCPTS Laboratory, Faculty of Electrical Engineering, U.S.T.H.B, Algiers, Algeria*
[2] *LCDEP Laboratory, Faculty of Electrical Engineering, U.S.T.H.B Univertsity, Algiers, Algeria*
[3] *EECS, University of Ottawa, Ottawa, Canada*

ABSTRACT: In this paper, an enhanced FDTD algorithm is proposed for an efficient characterization of HTS (high temperature superconductors) microwave planar filters. The developed algorithm, which can be generalized to any microwave planar circuit, is based on the two-fluid phenomenological model. Further, an irregular mesh discretization allowed improving the CPU time. Also, the thermal effects and normal conductivity have been rigorously taken into account for better performance. The impact of the operating temperature as well as the choice of the superconductor thickness was investigated. Computed results are in good agreement with simulated data using CST commercial software.

1. INTRODUCTION

Compared to conventional conductors, high temperature superconducting devices show some key advantages such as low dispersion and distortion, very low attenuation, and small losses in the design of passive devices such as interconnects, resonator filters, transmission lines, switches, couplers, and antennas [1–5]. Recently, high-temperature superconductors (HTSs) have become even more attractive in designing microwave filters because of their ultra-low losses and excellent out-of-band performances [3]. Furthermore, thanks to their low surface resistance compared to conventional materials, HTS resonator filters were produced with extremely low insertion losses and high-quality factor.

The development of simulation tools based on numerical models has become essential to predicting the thermal and electromagnetic (EM) behavior of high temperature superconductors, particularly in a precommercial stage of HTS structures. These numerical models have become an unavoidable tool thanks to the availability of relatively cost-effective computing tools. It also comes from the fact that the superconductor technology is becoming more and more widespread and is finding a variety of applications. On the other hand, predicting the EM behavior of such materials is not easy to simulate [6].

Several numerical approaches have been proposed to model superconducting materials like finite element method (FEM) [7–11], spectral domain approach (SDA) [12–15], integro-differential techniques [16, 17], RLC distributed model [18, 19], and finite-difference time-domain (FDTD) method [20–23].

In [7], the authors calculated the microwave surface resistance of HTS samples using the FEM based on the model proposed by Bonura et al. [8] and Coffey and Clem (CC) model. The dependence of the surface resistance versus the applied magnetic field was presented. COMSOL Multiphysics was then used to obtain the current distribution in the superconductor and the microwave surface resistance in the critical state. The results showed that for thin film low superconductor thicknesses, the predicted surface resistance value is considerably lower than those reported in the technical literature. This can be explained by the fact that the CC model is not applicable in this range of thickness values.

In [9] and [10], the FEM method was used to model the HTS material losses and current, while the superconductor was modeled with a power-law resistivity. In [11], another 2D FEM method based on the critical-state model was proposed to analyze HTS superconductors. In [12], the SDA method was proposed to model high superconductor films purity by using the CC unified theory where the surface impedance was evaluated as well as the propagation parameters depending on the operating temperature and the HTS thickness for three types of HTS quality. The complex conductivity of the superconductor was also evaluated versus magnetic field.

In [13], the Galerkin moment method was applied to model microstrip antennas with superconducting patches. Resonant frequency and half-power bandwidth were evaluated versus the operating temperature based on the two-fluid model and London's equations. The HTS thickness effect was also presented. In [14, 15], the propagation characteristics of a coplanar HTS waveguide, microstrip line, and slotline, using SDA approach, are reported. The superconductivity is introduced by the surface impedance of the HTS material based on modified two-fluid theory (from the Coffey and Clem model). The dispersion and attenuation parameters as well as the unloaded quality factor were evaluated versus the temperature and HTS thickness.

* Corresponding author: Mohamed Lamine Tounsi (mltounsi@ieee.org).

In [16], a 3D integro-differential model was developed and applied to compute the EM field of HTS composite materials, which are characterized by a nonlinear anisotropic electrical conductivity and multiscale dimensions. This model was formulated with the electric vector potential and discretization using the finite-difference method while in [17], a variational formulation has been adopted to model the superconductor. The EM problem was resolved using an integral formulation. In [18], RLC circuits were investigated to model the surface impedance R_s of HTS films. Linear, quadratic, and exponential dependence of R_s versus the RF magnetic field was simulated for a Hakki-Coleman dielectric resonator to study the nonlinear response of HTS material based on the modified two-fluid model. In [19], the authors studied the frequency-dependent RLGC electrical parameters of a high-speed HTS interconnect circuit, and an analysis response was proposed. A comparative simulation was carried out with normal conductors such as Aluminum (Al). The results showed that the crosstalk phenomenon was reduced with superconducting material.

In [20], an FDTD approach was applied to simulate a superconducting microstrip resonator. The resonant frequency was calculated versus the temperature using the kinetic inductance of the superconductor. In [21], FDTD approach was also used to model an HTS microstrip line based on Maxwell's equations and London theory. The effective dielectric constant, attenuation, supercurrent density distribution, and the magnetic field were evaluated. In [22], a 2D FDTD code with weighted Laguerre polynomials (WLP-FDTD) was applied to model microstrip superconducting lines with the advantage that the obtained algorithm is not restricted by the stability condition. In [23], a nonlinear phenomenological model of HTS material that combines the linear model of London equations and Ginzburg-Landau theory was proposed, leading to an empirical formula of the surface resistance of the superconductor with the use of YBCO (Yttrium barium copper oxide) as HTS material. The model was then applied to study the nonlinearity of an HTS filter.

One of the major problems encountered in the design of HTS microwave filters is the choice of the substrate which must have low losses on the whole operating frequency band and temperature. The substrate must also have a good resistance to mechanical stress during the transition to cryogenic temperature as well as a suitable crystalline mesh and a clean surface without defects [24, 25]. Another constraint with superconducting thin layers is compatibility criterion. Indeed, the cooling of the circuit to the cryogenic temperature causes a temperature difference about 220°K, so the materials undergo a thermal expansion more or less different. To quantify this phenomenon, one can define the coefficient of thermal expansion/dilatation (CTE) by [26, 27]:

$$k = \frac{\Delta l}{l_0 \Delta T} \tag{1}$$

with Δl being the variation of the length, ΔT the variation of temperature, and l_0 the initial length.

The coefficient k must be similar for the thin film HTS and substrate since the difference in CTE between the superconducting material and substrate can cause cracking during thermal cycling [28]. Another important parameter to take into consideration is the crystallographic property of the material. The lattice constant of the superconductor must be close to that of the substrate to allow epitaxy since the dielectric must not react with the components of the material HTS [29]. The values of the thermal expansion k and the lattice constant for different materials are reported in Table 1.

TABLE 1. Structural and thermal properties of selected substrate materials suitable for deposition of high-quality YBCO films [29].

	YBCO	MgO	$LaAlO_3$	Al_2O_3
Thermal expansion 10^{-6}/K	10–16	13–14	9	5–9
Lattice constant (nm)	0.382	0.421	0.379	0.348

Typically, the substrates that meet the mentioned criteria are Lanthanum aluminate ($LaAlO_3$), magnesium oxide (MgO), and sapphire (Al_2O_3) [29]. Lanthanum aluminate allows a good miniaturization, but the problem is related to its homogeneity that can affect the ability to set the frequency correctly, especially in narrow-band filter applications. This inhomogeneity can cause variations in the performance of the circuit [30, 31]. Magnesium oxide substrate (MgO) offers less miniaturization than Lanthanum aluminate but has satisfactory microwave properties with a loss tangent between $2 \cdot 10^{-6}$ and 10^{-5} at $T = 77\,\mathrm{K}$ and $f = 10\,\mathrm{GHz}$ [29]. The thermal expansion is compatible with YBCO thin films.

In this work, we highlight the materials and their characteristics for the design of HTS passive microwave circuits, in particular resonators and filters in planar technology. This design requires a precise the knowledge of materials properties and an in-depth study of their theory. An enhanced FDTD algorithm is therefore proposed to describe the superconducting material based on the two-fluid model and phenomenological model of superconductor in fullwave analysis. A coupled microstrip resonator is rigorously designed taking into account the thermal effect and HTS thickness.

2. MODELING OF HTS FILMS --- FDTD FORMALISM

2.1. London Theory --- Phenomenological Approach

Different theoretical approaches have been proposed to describe the properties of superconductors [32–35]. Gorter and Casimir [32] proposed a model to describe the thermodynamic properties of superconductors. In [35], London improved the two-fluid model by introducing the notion of penetration depth. In [34], Ginzburg and Landau showed that it is possible to describe the nonlinear behavior of superconductors by a macroscopic approach. Another more complete theory called BCS (Bardeen-Cooper-Schrieffer) was developed in [33] for low temperatures and used to interpret the superconducting phenomenon in HTS materials.

So, in the absence of a suitable and confirmed theory for the characterization of superconductivity at high critical tempera-

tures, scientists are trying to solve this problem using other approaches. The phenomenological model is indeed a quantitative description of microscopic properties [36]. As a general rule, the model is based on the two-fluid approach where conductivity σ is a complex quantity given by [37]:

$$\sigma = \sigma_n - j\sigma_s \tag{2}$$

where

$$\sigma_n = \sigma_c \cdot \left(\frac{T}{T_c}\right)^4 \tag{3a}$$

$$\sigma_s = \frac{1}{\omega\mu_0\lambda_L^2} \tag{3b}$$

where σ_n is the normal conductivity at critical temperature T_c, and λ_L, ω, and μ_0 are the London penetration depth, pulsation, and vacuum permeability.

The total current density is given as the sum of the normal current density $\overrightarrow{J_n}$ and the supercurrent density $\overrightarrow{J_s}$:

$$\vec{J} = \overrightarrow{J_n} + \overrightarrow{J_s} \tag{4}$$

This model introduces the concept of field penetration depth. It can be generally approximated by [36, 38, 39]

$$\left(\frac{\lambda_L(0)}{\lambda_L(T)}\right)^2 = 1 - \left(\frac{T}{T_c}\right)^{\Upsilon} \tag{5}$$

In the case of known superconductors such as Pb, Sn, or Nb, a good agreement with measurements was noted for $\Upsilon = 4$ [36, 40]. Note that from (3a), the normal conductivity σ_n at temperature T is always lower than the critical one σ_c at $T < T_c$. However, the measurements carried out on YBCO superconductors [41, 42] show that σ_n is larger than σ_c. A wide margin was observed between measured results and both classical two-fluid model and BCS theory [37]. Therefore, these two models are sufficient to explain the phenomenon of superconductivity at low temperature but are not applicable to HTS materials [43].

Another macroscopic model called enhanced two-fluid model was proposed in [43]. In this approach, parameter Υ depends on the superconductor films quality. In [36], Vendik et al. proposed a phenomenological model to describe the high temperature superconductors, where the empirical parameter Υ varies between 1.5 and 2.5. In addition, several experimental results show that HTS films have a parameter Υ value around 2 [38, 40].

From experimental results, three categories of HTS films were identified based on the superconductor quality: high, medium, or low purity films. This classification depends on the surface resistance properties [36, 38]. In [12], these three categories were highlighted and characterized by a phenomenological description of complex penetration depth, and the authors proposed a modeling methodology to analyze the HTS purity film by an EM wave propagation concept using a slotline configuration. Usually, for high quality YBCO parameter Υ is close to 2, while for poor YBCO quality, Υ tends to 1.5 [36].

Moreover, several empirical results show that the penetration depth at $T = 0°$K depends on the parameter Υ according to the following equation [38]:

$$\lambda_L(0) = 120 \cdot \exp(1.27 - 0.5\Upsilon) \text{ [nm]} \tag{6}$$

As mentioned before, since (3a) is incorrect for HTS thin films, and the validity range of (6) is restricted to LTS (low temperature superconductor) films. For the modified two-fluid model and for $T \leq T_c$, the following equation was then proposed [36, 39]:

$$\sigma_n(T) = \sigma_c \cdot \left(\frac{T}{T_c}\right)^{\Upsilon-1} + \alpha\left(1 - \left(\frac{T}{T_c}\right)^{\Upsilon}\right) \tag{7}$$

The empirical parameter α can be considered as the residual resistance that determines the value of the surface resistance at low temperatures [39]. Typically, α varies between 1 and 20 [36]. Note that for poor quality HTS thin films, the value of α is high (for example $\alpha = 15$ and $\Upsilon = 1.5$ [38]).

The surface resistance plays a fundamental role in the performance of superconductors for both passive and active components; it is the main parameter that indicates the material quality during the measurements and is defined as the ratio between transverse electric and magnetic fields relative to the surface [7].

In the case of HTS bulk samples which correspond to the case of HTS thicknesses t greater than twice of the London penetration depth ($t > 2\lambda_L$), the surface impedance is then given by [36, 39]:

$$Z_s = R_s + jX_s \tag{8}$$

where

$$R_s = \frac{1}{2}(\omega\mu_0)^2\sigma_n\lambda_L^3 \tag{9a}$$

$$X_s = \omega\mu_0\lambda_L \tag{9b}$$

If the thickness 't' of the superconducting film is less than twice of the London penetration depth ($t < 2\lambda_L$), one can use the following approximation [36, 39]:

$$R_s = (\omega\mu_0)^2\sigma_n\frac{\lambda_L^4}{t} \tag{10a}$$

$$X_s = \omega\mu_0\frac{\lambda_L^2}{t} \tag{10b}$$

2.2. FDTD Modeling of HTS Material

In this work, the FDTD approach has been used to resolve Maxwell's equations. Based on Yee notation (Fig. 1), the resolution of the partial derivative equations is performed in full-wave mode.

The proposed FDTD algorithm developed for modeling an HTS material uses an updated equation formulation. The electromagnetic (EM) field components are expressed at time $t_n = (n+1)\Delta t$, where Δt is the time step. The electric field is located by the mesh index (m, p, q) along the (x, y, z) directions

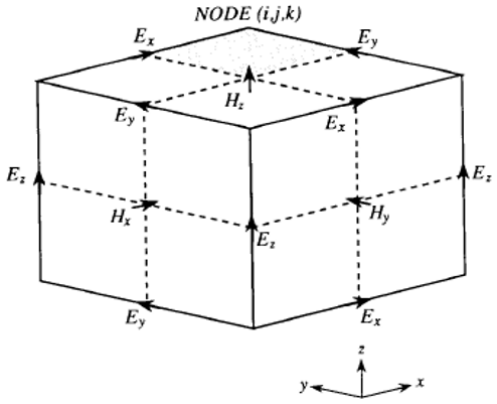

FIGURE 1. Field components in a Yee unit cell.

respectively. The tangential components of EM fields (parallel to the plane of the circuit) are [44]:

$$E_x^{n+1}\left(m+\frac{1}{2},p_s,q\right)=AE_x^s\cdot E_x^n\left(m+\frac{1}{2},p_s,q\right)$$
$$+E_{x1}^n\left(m,p_s,q\right)+E_{x2}^n\left(m,p_s,q\right)+E_{x3}^n\left(m,p_s,q\right) \quad (11a)$$

$$E_Z^{n+1}\left(m,p_s,q+\frac{1}{2}\right)=AE_Z^s\cdot E_Z^n\left(m,p_s,q+\frac{1}{2}\right)$$
$$+E_{z1}^n\left(m,p_s,q\right)+E_{z2}^n\left(m,p_s,q\right)+E_{z3}^n\left(m,p_s,q\right) \quad (11b)$$

where

$$E_{x1}^n\left(m,p_s,q\right)=BE_x^s\cdot\left[H_Z^{n+\frac{1}{2}}\left(m+\frac{1}{2},p_s+\frac{1}{2},q\right)\right.$$
$$\left.-H_Z^{n+\frac{1}{2}}\left(m+\frac{1}{2},p_s-\frac{1}{2},q\right)\right] \quad (12a)$$

$$E_{x2}^n\left(m,p_s,q\right)=CE_x^s\cdot\left[H_y^{n+\frac{1}{2}}\left(m+\frac{1}{2},p_s,q+\frac{1}{2}\right)\right.$$
$$\left.-H_y^{n+\frac{1}{2}}\left(m+\frac{1}{2},p_s,q-\frac{1}{2}\right)\right] \quad (12b)$$

$$E_{x3}^n\left(m,p_s,q\right)=DE_x^s\cdot\sum_{k=1}^{k=n}E_x^k\left(m+\frac{1}{2},p_s,q\right) \quad (12c)$$

$$E_{z1}^n\left(m,p_s,q\right)=BE_Z^s\cdot\left[H_y^{n+\frac{1}{2}}\left(m+\frac{1}{2},p_s,q+\frac{1}{2}\right)\right.$$
$$\left.-H_y^{n+\frac{1}{2}}\left(m-\frac{1}{2},p_s+\frac{1}{2},q\right)\right] \quad (12d)$$

$$E_{z2}^n\left(m,p_s,q\right)=CE_Z^s\cdot\left[H_x^{n+\frac{1}{2}}\left(m,p_s+\frac{1}{2},q+\frac{1}{2}\right)\right.$$
$$\left.-H_x^{n+\frac{1}{2}}\left(m,p_s-\frac{1}{2},q+\frac{1}{2}\right)\right] \quad (12e)$$

$$E_{z3}^n\left(m,p_s,q\right)=DE_Z^s\cdot\sum_{k=1}^{k=n}E_Z^k\left(m,p_s,q+\frac{1}{2}\right) \quad (12f)$$

The coefficients AE_i^s, BE_i^s, CE_i^s, and DE_i^s $(i=x,z)$ are given in [45]. p_s refers to the HTS interface index while t, λ_L, and σ_n represent the thickness films, London penetration depth, and normal conductivity, respectively. T and T_c are respectively the operating temperature and the critical temperature of the superconductor. Note that a refinement has been adopted using an irregular discretization [44].

2.3. Instability Problem and Time Incrementation

There are mainly two important criteria that must be respected in the FDTD numerical approach, namely, the numerical dispersion criterion and the choice of the time step. As far as the numerical dispersion is concerned, a spatial step must be chosen sufficiently small, in the band corresponding to $[\lambda_{\min},\lambda_{\max}]$, according to:

$$\text{Max}\left\{\Delta_x\left(m\right),\Delta_y\left(p\right),\Delta_Z\left(q\right)\right\}\leq\frac{\lambda_{\min}}{20} \quad (13)$$

with $\lambda_{\min}$ being the minimum wavelength of the propagated wave.

In the case of standard FDTD formulation involving dielectric/magnetic linear media, the time increment step is not arbitrary, and an upper limit must be set to avoid overflow problem. This limit is fixed by the CFL (Current-Friedrichs-Lewy) condition [45]:

$$\Delta t\leq\frac{1}{V_{\max}\sqrt{\frac{1}{\Delta x^2}+\frac{1}{\Delta y^2}+\frac{1}{\Delta z^2}}} \quad (14)$$

$$V_{\max}=\frac{C}{\sqrt{\mu_r\varepsilon_r}} \quad (15)$$

$V_{\max}$ is the maximal speed of the propagated wave; C is the speed of light; ε_r and μ_r are the relative permittivity and permeability, respectively.

However, in a superconductor region, the CFL conditions are not applicable. There are no known criteria for the choice of Δt for this type of material, and it is necessary to consider a step Δt lower than the one imposed by CFL.

As in [20], we considered two kinds of time increments (i) Δt that meets the CFL criterion, with the spatial region being the volume of the structure that includes the substrate and upper layer, (i.e., the air), to which the superconductor region is restricted, and (ii) Δt_0 only dedicated to the HTS films spatial region and given such as:

$$\Delta t=i\Delta t_0,\quad i\in N \quad (16)$$

3. STUDY OF THE HTS RESONATOR PERFORMANCE

In this section, the performances of an HTS microwave coupled resonator (Fig. 2) are analyzed. The HTS thermal and thickness effects on resonance frequency, insertion losses, and bandwidth are investigated. The physical dimensions of the coupled resonator are reported in Table 2 [20].

The resonator is etched on two layers: the bottom layer is a dielectric material MgO with $\varepsilon_r=8.5$. The top layer is a microstrip pattern of YBCO films with $T_c=88\,\text{K}$, $\sigma_c=2.7\cdot10^6\,(\text{s/m})$, $\alpha=3.1$, and $\Upsilon=1.95$. The bottom and upper

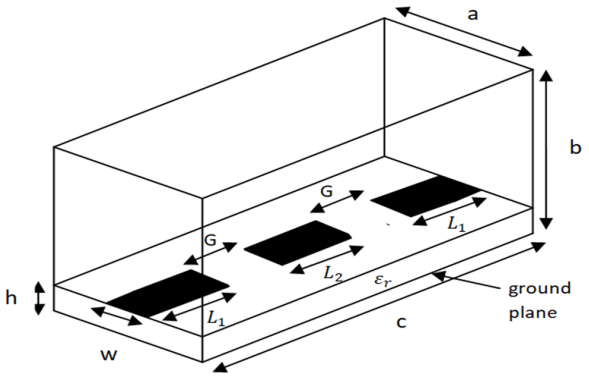

FIGURE 2. The HTS coupled microstrip resonator [20].

TABLE 2. Dimensions of the HTS coupled resonator [20].

	a	b	c	G	W	L_1	L_2	h
Dimensions (mm)	5	5	10	0.5	0.5	2.5	4	0.5

parts of the structure as well as the side parts are delimited by perfectly electric conductors (PECs) ($E_{tg} = 0$). Two walls with first order Mur condition (absorbing condition of Mur) are placed at $z = 0$ and $z = c$ in order to eliminate the effect of parasitic reflections. The waveform excitation is a Gaussian signal, and the pulse width is chosen small enough to cover the band [0–15 GHz].

3.1. Effect of the HTS Thickness

The operating temperature is fixed at $T = 77°$K. As shown in Figs. 3, 5, 6 for the transmission coefficient (S_{21}) and Figs. 4, 7, 8 for the refection coefficient (S_{11}) at different thicknesses, the computed results are in good agreement with those simulated with CST EM tool. The modeling of the HTS film under the CST simulator is carried out using the surface impedance procedure depending on the thickness t value.

Figure 9 illustrates the variation of the parameter $\frac{t}{\lambda_L}$ versus t at $T = 77°$K. According to (5) and (6), the London penetration depth is evaluated as $\lambda_L = 336.62$ nm. Therefore, the HTS material is considered as bulk samples for thicknesses exceeding 673 nm and as thin film in the other case. Let us recall that according to the Vendik model, the superconducting material is considered as thin films for a thickness less than $2\lambda_L(\frac{t}{\lambda_L} < 2)$, and is considered as bulk sample in the other case.

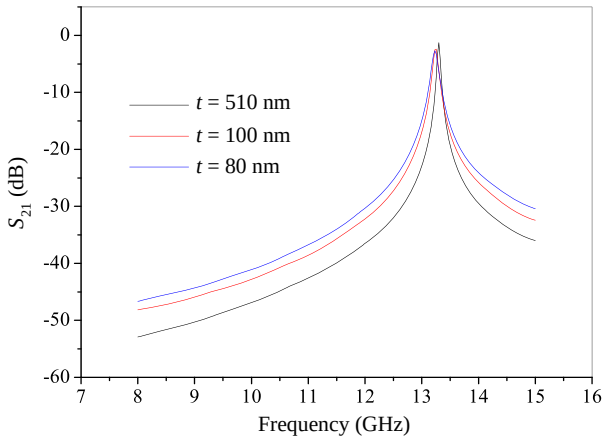

FIGURE 3. S_{21} parameter versus frequency for different thicknesses.

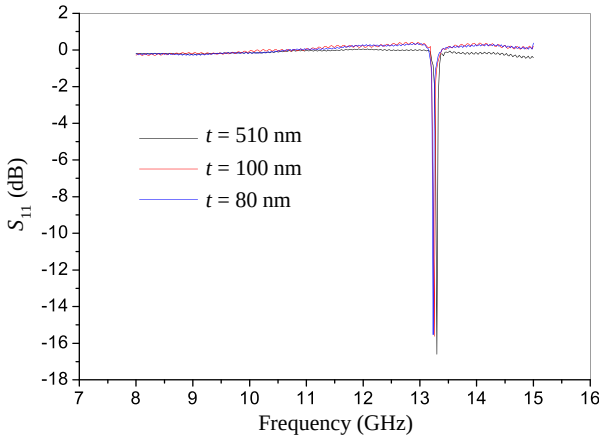

FIGURE 4. S_{11} parameter versus frequency for different thicknesses.

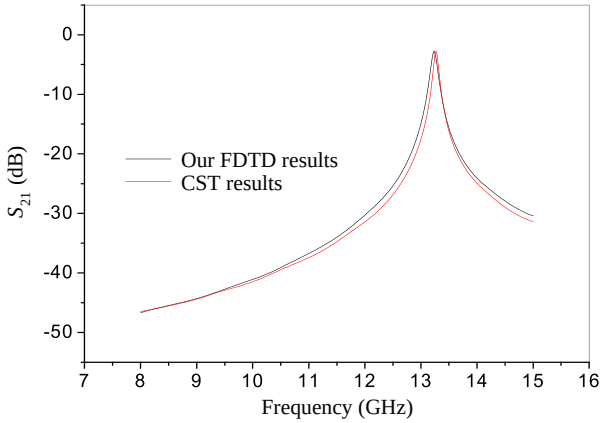

FIGURE 5. S_{21} parameter versus frequency for $t = 80$ nm.

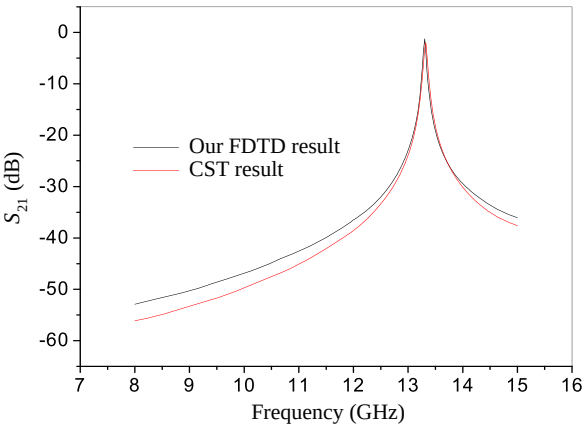

FIGURE 6. S_{21} parameter versus frequency for $t = 510$ nm.

Figures 10–12 show the variation of the structure parameters vs. the HTS thicknesses at $T = 77$ K. As shown in Fig. 10, the insertion losses (IL) is maximum for low values of t, with a relatively constant value from 505 nm (about $1.5\lambda_L$). This phenomenon has already been demonstrated in the case of nor-

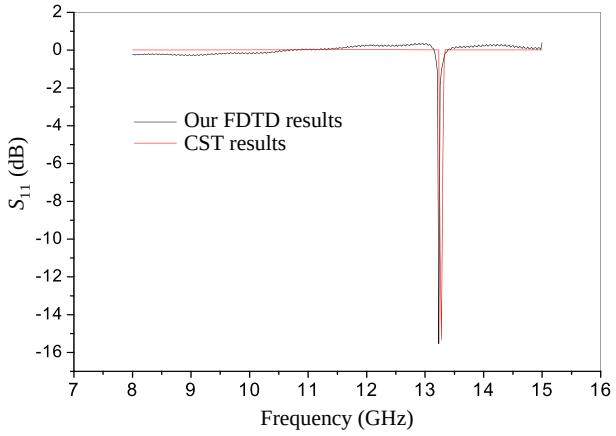

FIGURE 7. S_{11} parameter versus frequency for $t = 80$ nm.

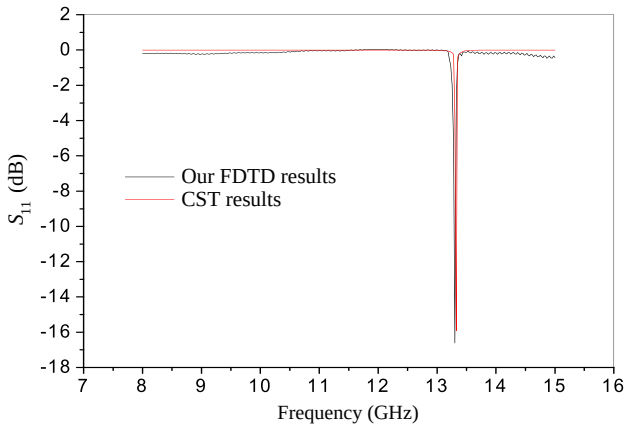

FIGURE 8. S_{11} parameter versus frequency for $t = 510$ nm.

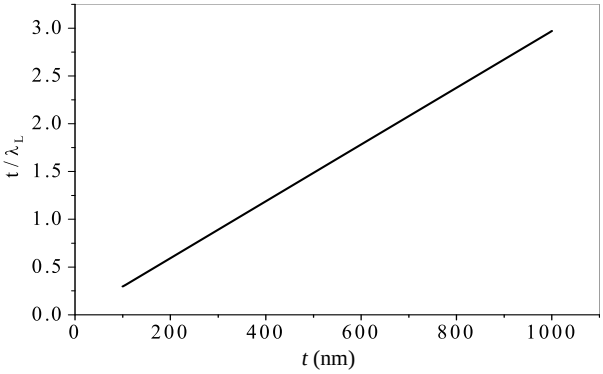

FIGURE 9. Variation of $\frac{t}{\lambda_L}$ versus t.

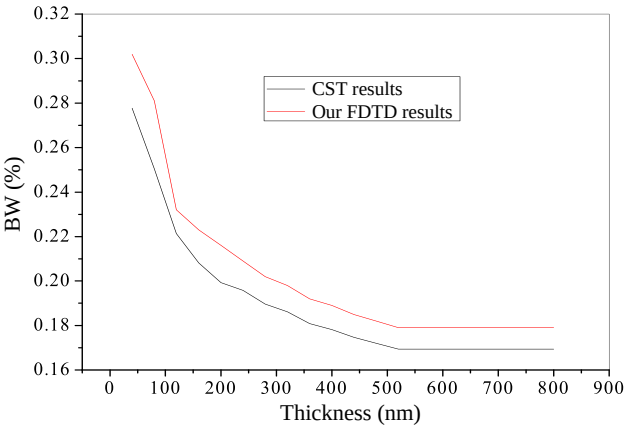

FIGURE 11. Variation relative bandwidth versus the thickness of superconductor at $T = 77$ K.

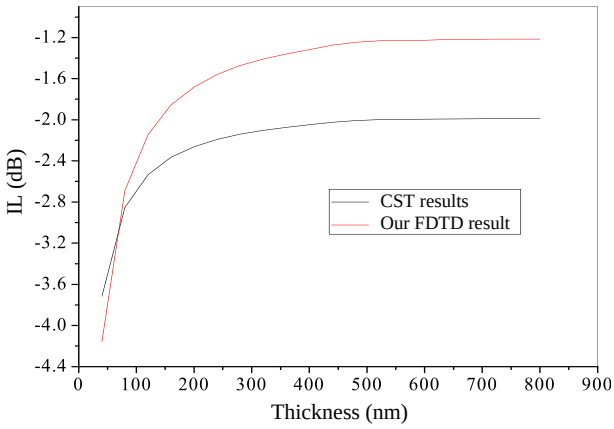

FIGURE 10. Variation insertion losses versus the thickness of superconductor at $T = 77$ K.

mal conductors [46, 47]. In [12], the attenuation coefficient of an HTS microstrip line was evaluated using the spectral domain approach (SDA) method; the superconducting material was modeled by its surface impedance; and the results showed that the attenuation tended to increase for low values of t. The attenuation of a microstrip line was related to the losses by joule effect. The result demonstrates that for the low values of the thickness of the HTS film, the losses in the material increase, which implies more insertion losses. This analysis shows that the choice of the thickness t is important for the design process, and an unwise choice can lead to significant losses causing a degradation of the filter performance.

In Fig. 11, the relative bandwidth (BW) decreases drastically for low values of t and then becomes almost constant from the same t value ($t = 505$ nm). A sudden threshold effect is reported showing that the resonator becomes more selective with a maximum quality factor. This coincides also with a minimal IL in this range. This variation is explained by the fact that the unloaded quality factor (inverse of the relative band) is inversely proportional to the losses in the resonator.

As for Fig. 12, it is shown that the resonance frequency f_0 follows almost the same behavior: it increases with t until $1.5\lambda_L$ before converging to a constant value.

Our result predicts a shift in resonance frequency depending on the thickness of the HTS film.

To explain this resonance phenomenon, it is known that independent of the shape of the resonator, it is possible to model it by an RLC network where the resonance frequency can be evaluated as:

$$f_0 = \frac{1}{\sqrt{LC}} \tag{17}$$

L and C represent respectively the equivalent inductance and capacity of the resonator. For HTS microstrip lines, the equivalent inductance is mainly due to the kinetic inductance (eval-

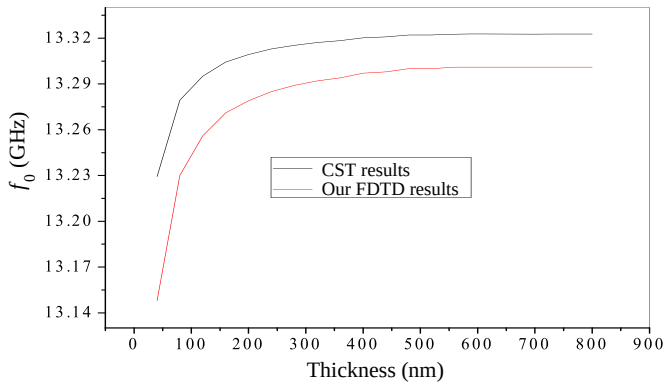

FIGURE 12. Variation of resonance frequency versus the thickness of superconductor at $T = 77°$K.

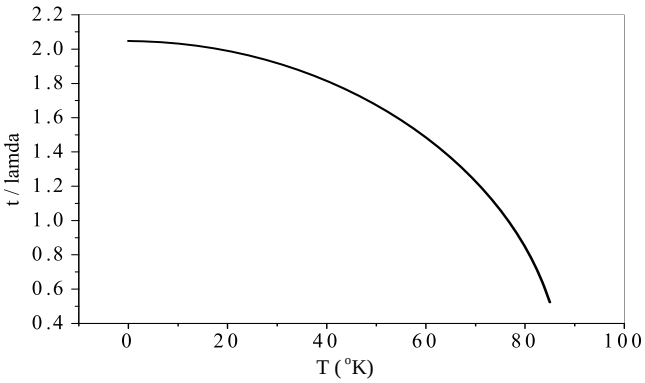

FIGURE 14. Variation of $\frac{t}{\lambda_L}$ versus T.

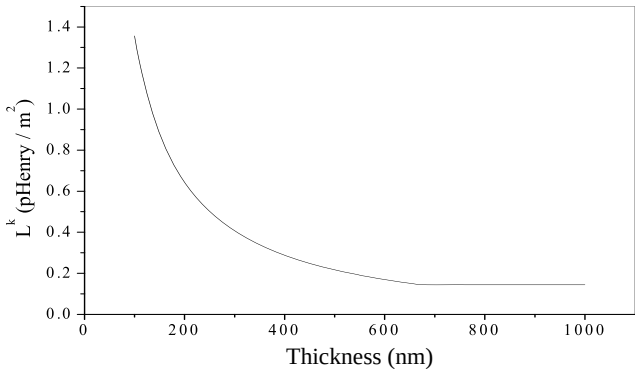

FIGURE 13. Variation of kinetic inductance versus the thickness of HTS films.

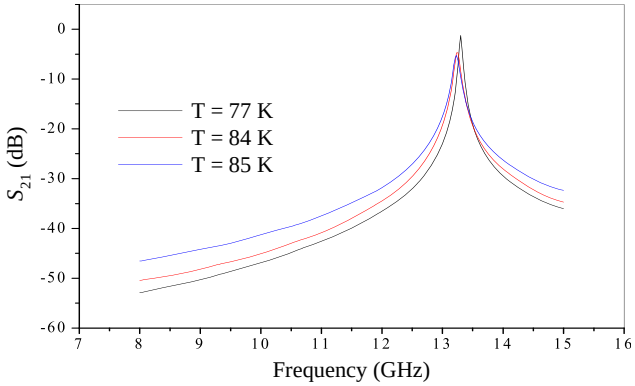

FIGURE 15. S_{21} parameter versus frequency for different operating temperatures.

uated using the transport properties of charge carriers in the superconducting parts of the resonator) while its geometry depends on the external magnetic field [36, 48–50]. The surface kinetic inductance can be deduced from (9b) and (10b) as [36]:

$$x_{sur} = wL^k \tag{18}$$

From (18), we can obtain the variation of the kinetic inductance L^k versus HTS thickness. Fig. 13 illustrates this variation where a decrease in the kinetic inductance is observed versus t. Since the resonant frequency is proportional to the inverse of the inductance root, we can explain the variation of f_0 in Fig. 12. This analysis shows the need to take into account the thickness of the superconductor in any design process; otherwise, large offsets can occur in the resonant frequency. A good agreement was obtained in comparison with the CST results with an average relative error of 6%, 7%, and 0.21%, respectively for relative band, insertion losses, and the resonant frequency.

3.2. Effect of the Operating Temperature

In this study, the HTS thickness is fixed at $t = 510$ nm. First, we note that according to the phenomenological model proposed by Vendik et al. [36], the surface impedance Z_s depends on the ratio t/λ_L (thin films and bulk sample case), and the ratio depends on the operating temperature (Fig. 14). So, we must use the adequate formula of Z_s according to the operating temperature.

The operating temperature is fixed to $T = 77$ K. As shown in Figs. 15, 17, 18 for the transmission coefficient (S_{21}) and Figs. 16, 19, 20 for the refection coefficient (S_{11}) at different thicknesses, the computed results are in good agreement with those simulated with CST EM tool. The modeling of the HTS film under the CST simulator is carried out using the surface impedance procedure depending on the thickness t value.

After simulating the structure at different values of the operating temperature T, we obtained the curves illustrated in Figs. 21, 22, and 23.

Figure 21 gives the variation of the insertion losses (IL) versus T at $t = 510$ nm. We can observe a progressive decrease of IL for temperatures ranging from 0 to 75 K before decreasing dramatically. This can be explained physically: at temperatures below the transition temperature T_c and according to the two-fluid model, the normal electrons behave like super-electrons; therefore, all the current is carried by them. However, by increasing the temperature, a part of the current is carried by the normal electrons which causes collisions in the material and then in power losses. Approaching T_c, most of the electrons become normal, and the material loses its superconductivity. Several studies have highlighted this phenomenon [12, 36, 51]. Note that the obtained results are in good agreement with those simulated by CST software tool.

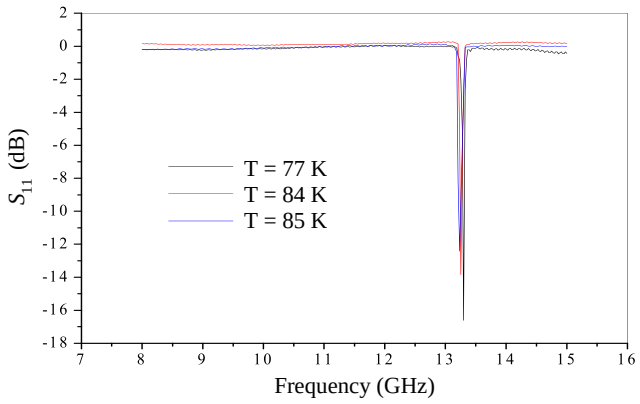

FIGURE 16. S_{11} parameter versus frequency for operating temperature.

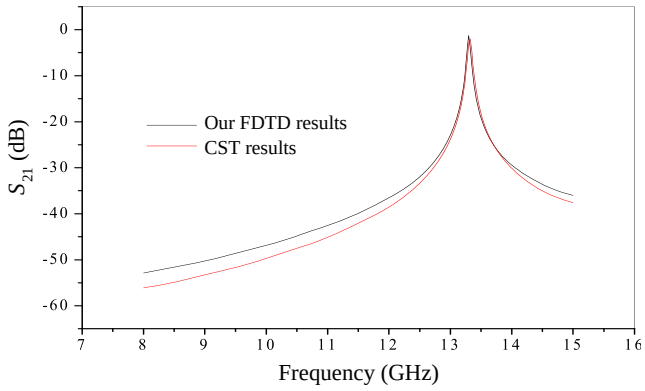

FIGURE 17. S_{21} parameter versus frequency for $T = 77\,\text{K}$.

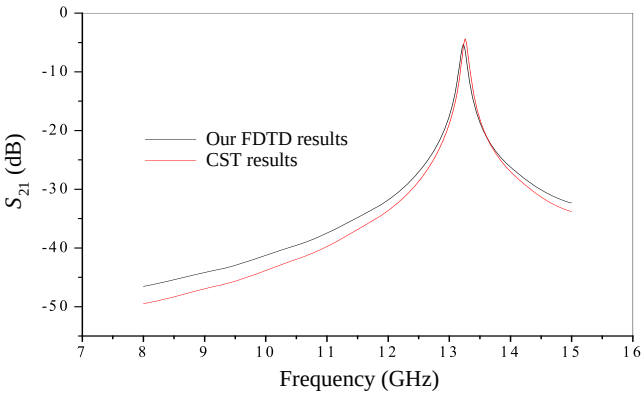

FIGURE 18. S_{21} parameter versus frequency for $T = 85\,\text{K}$.

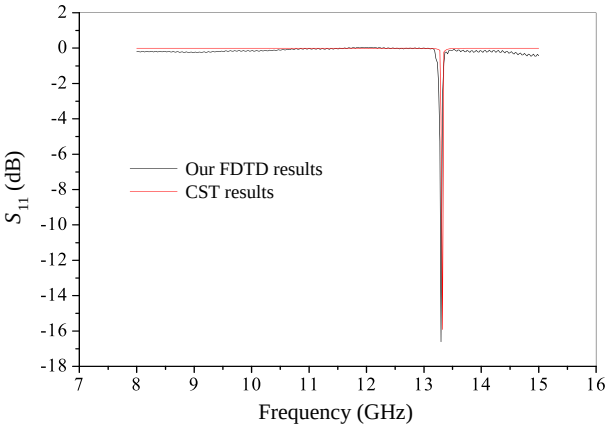

FIGURE 19. S_{11} parameter versus frequency for $T = 77\,\text{K}$.

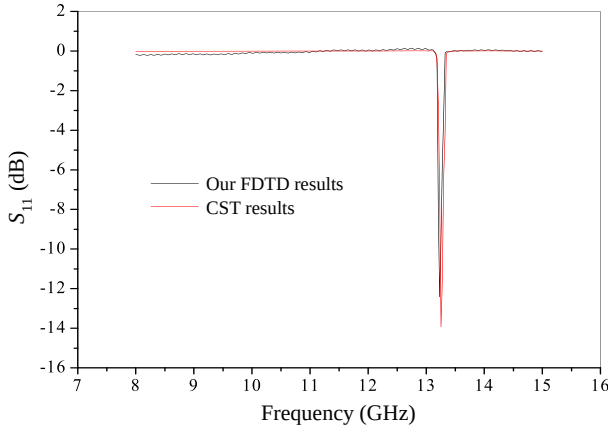

FIGURE 20. S_{11} parameter versus frequency for $T = 85\,\text{K}$.

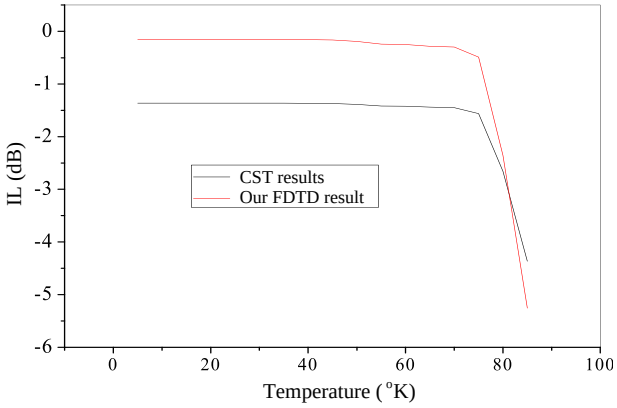

FIGURE 21. Variation of insertion loss versus T at $t = 510\,\text{nm}$.

Figure 22 gives the variation of relative bandwidth (BW) versus T at $t = 510\,\text{nm}$. Note that BW is independent of the temperature from $T < 75\,\text{K}$, then a significant increase appears before being maximum near the critical temperature due to the presence of a significant proportion of normal electrons. Thus, the quality factor is better for low temperatures with minimal insertion losses in this temperature range.

The variation of BW can be explained by Fig. 21 (because the unloaded quality factor is inversely proportional to the losses in a resonator), and this observation has already been underlined in other works [13, 52]. A good agreement was obtained in comparison with the CST results with an average relative error of 9%, 13%, and 0.11%, respectively for relative band, insertion loss, and resonant frequency.

Figure 23 gives the variation of the resonance frequency f_0 versus T at $t = 510\,\text{nm}$. A progressive decrease of the resonance frequency is reported for T in the range 0–75 K. This decrease is greater near the transition temperature. A good

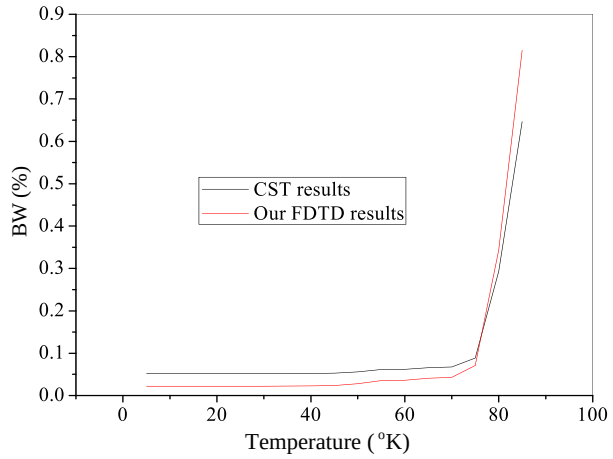

FIGURE 22. Variation of relative band versus operating temperature of superconductor at $t = 510\,\text{nm}$.

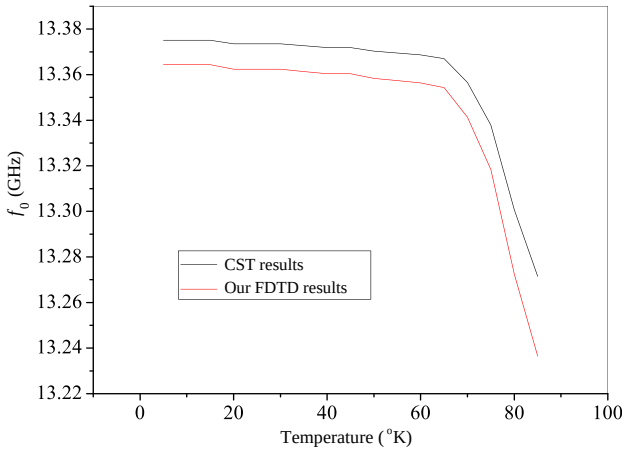

FIGURE 23. Variation of resonance frequency versus operating temperature of superconductor at $t = 510\,\text{nm}$.

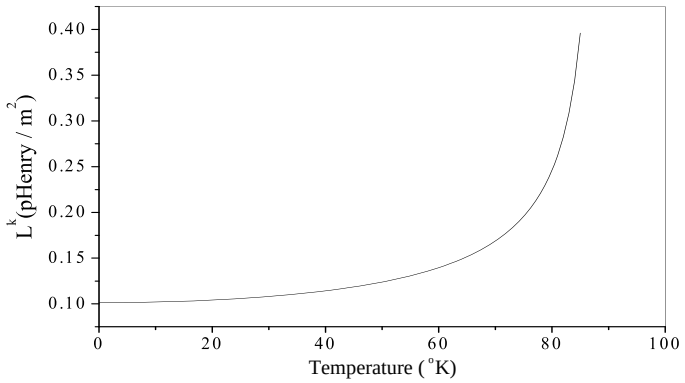

FIGURE 24. Variation of the kinetic inductance versus the operating temperature T at $t = 510\,\text{nm}$.

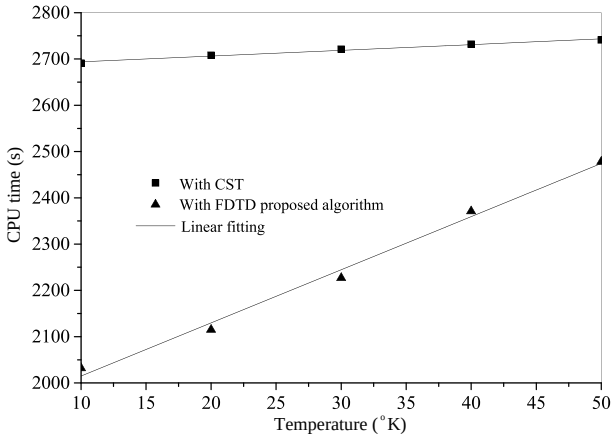

FIGURE 25. CPU time versus temperature T.

agreement is observed with regard to CST simulations, with an average relative error that does not exceed 0.1%. This phenomenon is similar to that observed in Fig. 12 based on the RLC model (Equation (17)). We can then deduce that the variation of f_0 is determined by that of kinetic inductance. Note that the measured resonant frequency shows an increase with temperature [50], and this phenomenon is attributed to the kinetic inductance. Using (9b), (10b), and (18), we plotted the variation of f_0 versus T (Fig. 24).

This study shows a significant dependence of the resonant frequency f_0 vs. the temperature, especially close to the transition temperature. Hence, the HTS material cannot be simply modeled by a perfectly conductive material (PEC). This illustrates the importance of the model describing the superconductor while the temperature dependence is taken into account.

As already mentioned, since the proposed enhanced algorithm considers an irregular discretization, it allows improving the CPU time. Next, the superconducting material was introduced rigorously via an in-depth study based on the phenomenological two-fluid approach taking into account the HTS thin film as well as the thermal dependence of the filter performance.

Figure 25 illustrates the CPU time of the proposed FDTD algorithm with regard to the one obtained with CST at different temperatures (with $t = 800\,\text{nm}$) showing a considerable CPU time saving particularly for low temperatures. Note also that the CPU time increases linearly versus temperature which is confirmed by the linear fitting in both computed and simulated data using the proposed FDTD algorithm and CST tool respectively.

4. CONCLUSION

In this work, a new FDTD algorithm with nonuniform mesh discretization is proposed to describe high temperature superconductor (HTS) based on a two-fluid phenomenological model. The developed update equations can be applied to analyze a spectral behavior of planar microwave circuit based on HTS material. The thermal effects as well as the impact of thickness HTS films on the resonator performances were also investigated; we have highlighted the importance of the choice of the thickness of the HTS thin film. Our investigation showed that it is suitable to use a thickness about 1.5 times of the London penetration depth to reduce the insertion losses and increase the resonator selectivity. A relatively large shift of the resonance

frequency was reported versus HTS thickness. This denotes the necessity to taking into account the HTS thickness to avoid errors in the design process. The effect of temperature was studied too. The computed results have shown a significant improvement in the resonator performance at low temperature: the insertion losses were minimized and the selectivity improved. Furthermore, the obtained results show a strong dependence on the performance of the filter for temperatures close to the critical temperature. This highlights the importance of the chosen model to describe the HTS thin films, for filter design. The proposed approach was demonstrated through close agreement with CST simulated data. Note that the proposed model can be improved in the future work by including the magnetic field dependence of the London penetration depth and, thus, the nonlinear character of the superconductor. The precision can also be improved by adopting other absorption conditions in the FDTD algorithm, especially perfectly matched layers (PMLs).

ACKNOWLEDGEMENT

This work was supported by the Ministry of Higher Education and Scientific Research of Algeria and the Faculty of Electrical Engineering, USTHB University, Algiers, Algeria.

REFERENCES

[1] Tounsi, M. L., O. Madani, M. Bensebti, and M. C. E. Yagoub, "FDTD analysis of shielding in high-Tc microstrip resonators on anisotropic substrates," in *European Electromagnetics Symposium (EUROEM 2012)*, Toulouse, France, Jul. 2012.

[2] Tounsi, M. L., A. Belguidoum, and M. C. E. Yagoub, "Hybrid-mode analysis of anisotropic high-Tc superconducting passive microwave circuits on lossy anisotropic dielectric layers," in *2011 Saudi International Electronics, Communications and Photonics Conference (SIECPC)*, 1–4, Saudi Arabia, Apr. 2011.

[3] Liu, H., B. Ren, S. Hu, X. Guan, P. Wen, and J. Tang, "High-order dual-band superconducting bandpass filter with controllable bandwidths and multitransmission zeros," *IEEE Transactions on Microwave Theory and Techniques*, Vol. 65, No. 10, 3813–3823, Oct. 2017.

[4] Rietschel, H., "High-Tc superconductivity: Present status of fundamental research and applications," *Active and Passive Electronic Components*, Vol. 15, No. 3-4, 111–116, 1993.

[5] Dymnikov, A. A. and O. D. Poustylnik, "Use of the phenomenon of high-temperature superconductivity for the creation of integrated devices of microwave electronics," *International Journal of Infrared and Millimeter Waves*, Vol. 20, No. 5, 937–965, 1999.

[6] Grilli, F., "Numerical modeling of HTS applications," *IEEE Transactions on Applied Superconductivity*, Vol. 26, No. 3, 1–8, Apr. 2016.

[7] Yildiz, S., F. Inanir, and A. Cicek, "A novel method for numerical analysis of microwave surface resistance of type-II superconductors," *IEEE Transactions on Applied Superconductivity*, Vol. 26, No. 2, 1–5, Mar. 2016.

[8] Bonura, M., A. A. Gallitto, and M. LiVigni, "Magnetic hysteresis in the microwave surface resistance of nb samples in the critical state," *Eur. Phys. J. B*, Vol. 53, No. 3, 315–322, Oct. 2006.

[9] Maslouh, M., F. Bouillault, and J. C. Verite, "Two-dimensional numerical modeling of superconductors with imposed currents by the finite element method," *IEEE Transactions on Magnetics*, Vol. 36, No. 4, 1234–1237, Jul. 2000.

[10] Amemiya, N., S.-I. Murasawa, N. Banno, and K. Miyamoto, "Numerical modelings of superconducting wires for AC loss calculations," *Physica C: Superconductivity*, Vol. 310, No. 1-4, 16–29, Dec. 1998.

[11] Ruiz-Alonso, D., T. A. Coombs, and A. M. Campbell, "Numerical analysis of high-temperature superconductors with the critical-state model," *IEEE Transactions on Applied Superconductivity*, Vol. 14, No. 4, 2053–2063, Dec. 2004.

[12] Andrews, J., S. P. Chakyar, V. P. Joseph, and V. Mathew, "Spectral domain modeling of the effect of film purity for superconducting slotline," in *2016 IEEE MTT-S International Conference on Numerical Electromagnetic and Multiphysics Modeling and Optimization (NEMO)*, 1–3, Beijing, China, Jul. 2016.

[13] Fortaki, T., M. Amir, S. Benkouda, and A. Benghalia, "Study of high Tc superconducting microstrip antenna," *PIERS Online*, Vol. 5, No. 4, 346–349, 2009.

[14] Andrews, J. and V. Mathew, "Computation of flux effects in high temperature superconducting coplanar waveguide," in *2014 International Conference on Numerical Electromagnetic Modeling and Optimization for RF, Microwave, and Terahertz Applications (NEMO)*, 1–4, Pavia, Italy, May 2014.

[15] Andrews, J. and V. Mathew, "Modeling of frequency response in vortex state of high temperature superconducting microstrip and slotline," in *2015 IEEE MTT-S International Conference on Numerical Electromagnetic and Multiphysics Modeling and Optimization (NEMO)*, 1–4, Ottawa, ON, Canada, Aug. 2015.

[16] Menana, H., M. Farhat, M. Hinaje, and B. Douine, "An integro-differential time-domain scheme for electromagnetic field modeling in HTS materials," *IEEE Transactions on Magnetics*, Vol. 56, No. 3, 1–4, Mar. 2020.

[17] Rubinacci, G., A. Tamburrino, and F. Villone, "Three dimensional finite elements modeling of superconductors," *IEEE Transactions on Magnetics*, Vol. 36, No. 4, 1276–1279, Jul. 2000.

[18] Ledenyov, D., J. Mazierska, G. Allen, and M. Jacob, "Lumped element modeling of nonlinear properties of high temperature superconductors in a dielectric resonator," in *15th International Conference on Microwaves, Radar and Wireless Communications (IEEE Cat. No. 04EX824)*, Vol. 3, 824–827, Warsaw, Poland, May 2004.

[19] Mao, J.-F., X. Qian, and Z. Yuan, "Characteristic analysis of coupled HTS interconnects with two-dimensional FDTD," *IEEE Microwave and Wireless Components Letters*, Vol. 11, No. 1, 33–35, Jan. 2001.

[20] Okazaki, Y., K. Suzuki, and Y. Enomoto, "Superconducting microstrip resonator investigated by FDTD electromagnetic field simulator," *IEEE Transactions on Applied Superconductivity*, Vol. 9, No. 2, 3034–3037, Jun. 1999.

[21] Ghamlouche, H., M. Benkraouda, M. Hussein, and T. Badarneh, "Microwave characterization of high-Tc superconducting microstrip line using FDTD technique," in *2006 Asia-Pacific Microwave Conference*, 1268–1271, Yokohama, Japan, Dec. 2006.

[22] Li, Y., X. Li, and J. Mao, "A compact 2-D WLP-FDTD method for superconducting microstrip lines," in *2018 Asia-Pacific Microwave Conference (APMC)*, 636–638, Kyoto, Japan, Nov. 2018.

[23] Megahed, M., S. El-Ghazaly, and A. Fathy, "Analysis of HTS filters using novel nonlinear phenomenological two fluid model," in *1996 IEEE MTT-S International Microwave Symposium Digest*, Vol. 3, 1497–1500, San Francisco, CA, USA, Jun. 1996.

[24] Jacob, M. V., J. Mazierska, N. Savvides, S. Ohshima, and S. Oikawa, "Comparison of microwave properties of YBCO films on MgO and $LaAlO_3$ substrates," *Physica C: Supercon-*

ductivity, Vol. 372-376, 474–477, Aug. 2002.

[25] Schneider, R., R. Aidam, A. Zaitsev, J. Geerk, G. Linker, F. Ratzel, and R. Smithey, "Resonators and filters made of YBaCuO thin films on sapphire wafers," *Physica C: Superconductivity*, Vol. 351, No. 1, 21–24, Mar. 2001.

[26] Oeschler, N., P. Gegenwart, F. Steglich, N. A. Frederick, E. D. Bauer, and M. B. Maple, "Thermal expansion of the skutterudite superconductor $PrOs_4Sb_{12}$," *Acta Physica Polonica Series B*, Vol. 34, No. 2, 959, Feb. 2003.

[27] Lortz, R., Y. Wang, S. Abe, C. Meingast, Y. B. Paderno, V. Filippov, and A. Junod, "Specific heat, magnetic susceptibility, resistivity and thermal expansion of the superconductor ZrB_{12}," *Physical Review B*, Vol. 72, No. 2, 024547, Jul. 2005.

[28] Chandran, B., R. C. Goforth, and S. Nasrazadani, "Measurement of the coefficient of thermal expansion of superconducting thin films using powder X-ray diffraction," *Journal of the Arkansas Academy of Science*, Vol. 46, No. 1, 39, 1992.

[29] Hein, M., *High-Temperature-Superconductor Thin Films at Microwave Frequencies*, Springer Science & Business Media, 1999.

[30] Mansour, R. R., "Microwave superconductivity," *IEEE Transactions on Microwave Theory and Techniques*, Vol. 50, No. 3, 750–759, Mar. 2002.

[31] Andreone, A., A. Cassinese, M. Iavarone, P. Orgiani, F. Palomba, G. Pica, M. Salluzzo, and R. Vaglio, "Development of L-band and C-band superconducting planar filters for wireless systems," in *2000 Asia-Pacific Microwave Conference. Proceedings (Cat. No. 00TH8522)*, 581–586, Sydney, NSW, Australia, 2000.

[32] Gorter, C. and H. Casimir, "On the thermodynamics of the superconducting state," *Journal of Physics*, Vol. 35, 963–966, 1934.

[33] Bardeen, J., L. N. Cooper, and J. R. Schrieffer, "Theory of superconductivity," *Physical Review*, Vol. 108, No. 5, 1175–1204, 1957.

[34] Ginzburg, V. L. and L. D. Landau, "To the theory of superconductivity," *Journal of Exerimental and Theoretical Physics*, Vol. 20, No. 1064-1082, 1950.

[35] London, F. and H. London, "The electromagnetic equations of the supraconductor," in *Proceedings of the Royal Society, A: Mathematical, Physical and Engineering Sciences*, Vol. 149, No. 866, United Kingdom, Mar. 1935.

[36] Vendik, O. G., I. B. Vendik, and D. I. Kaparkov, "Empirical model of the microwave properties of high-temperature superconductors," *IEEE Transactions on Microwave Theory and Techniques*, Vol. 46, No. 5, 469–478, May 1998.

[37] Ma, J.-G. and I. Wolff, "Electromagnetics in high-T/sub c/ superconductors," *IEEE Transactions on Microwave Theory and Techniques*, Vol. 44, No. 4, 537–542, Apr. 1996.

[38] Vendik, I. B., "Phenomenological model of the microwave surface impedance of high-Tc superconducting films," *IEEE Transactions on Applied Superconductivity*, Vol. 11, No. 1, 3545–3548, Mar. 2001.

[39] Vendik, O. G., I. B. Vendik, and D. V. Kholodniak, "Applications of high-temperature superconductors in microwave integrated circuits," *Mater. Phys. Mech*, Vol. 2, 15–24, Jan. 2000.

[40] Wu, C.-J. and Y.-L. Chen, "Microwave properties of a high-temperature superconductor and ferromagnetic bilayer structure," *Progress In Electromagnetics Research*, Vol. 111, 433–445, 2010.

[41] Bhasin, K. B., J. D. Warner, F. A. Miranda, W. L. Gordon, and H. S. Newman, "Determination of surface resistance and magnetic penetration depth of superconducting $YBa_2Cu_3/O_{7-\delta}$ thin films by microwave power transmission measurements," *IEEE Transactions on Magnetics*, Vol. 27, No. 2, 1284–1287, 1991.

[42] Piel, H. and G. Muller, "The microwave surface impedance of high-Tc superconductors," *IEEE Transactions on Magnetics*, Vol. 27, No. 2, 854–862, 1991.

[43] Kobayashi, Y., "Microwave applications of high-temperature superconductor devices," in *1996 26th European Microwave Conference*, Vol. 2, 823–829, Prague, Czech Republic, 1996.

[44] Laoufi, M. K., S. Mekaoui, and M. L. Tounsi, "HTS dual-filters for WLAN and 4G applications," in *2020 IEEE Asia-Pacific Microwave Conference (APMC)*, 740–742, Hong Kong, 2020.

[45] He, X., B. Wei, and K. Fan, "A hybrid FDTD algorithm without the limitation of CFL condition," in *2019 IEEE International Conference on Computational Electromagnetics (ICCEM)*, 1–2, Shanghai, China, 2019.

[46] Vietzorreck, L. and W. Pascher, "Influence of conductor loss and thickness in coplanar circuit elements," in *1997 IEEE MTT-S International Microwave Symposium Digest*, Vol. 3, 1811–1814, Denver, CO, USA, 1997.

[47] Singh, P. and A. K. Verma, "Analysis of multilayer microstrip line of finite conductor thickness using quasi-static spectral domain analysis (SDA) and single layer reduction (SLR) method," in *2011 Annual IEEE India Conference*, 1–4, Hyderabad, India, 2011.

[48] Cai, H., H. Li, E. Y. Cho, and S. A. Cybart, "Inductance of $YBa_2Cu_3O_{7-\delta}$ thin-films with and without superconducting ground planes," *IEEE Transactions on Applied Superconductivity*, Vol. 30, No. 7, 1–5, Jun. 2020.

[49] Ha, D.-G., S. H. Kim, S.-Y. Jun, S. B. Shim, W. Song, J. H. Park, J. Choi, and Y. Chong, "Development of high quality superconducting resonators for quantum device applications," in *2013 IEEE 14th International Superconductive Electronics Conference (ISEC)*, 1–3, Cambridge, MA, Jul. 2013.

[50] Trang, F., H. Rogalla, and Z. Popović, "Resonant response of high-temperature superconducting split-ring resonators," *IEEE Transactions on Applied Superconductivity*, Vol. 23, No. 3, 1300405, Jun. 2013.

[51] Deleniv, A., T. Martinsson, and I. Vendik, "CAD model of high-Tc superconducting coplanar waveguide resonator on isotropic and anisotropic substrate," in *1996 26th European Microwave Conference*, Vol. 1, 510–513, Prague, Czech Republic, Sep. 1996.

[52] Vendik, I., S. Gevorgian, D. Kaparkov, and A. Monin, "High-Tc superconductor microstrip resonator on sapphire substrate (R-cut)," in *1995 25th European Microwave Conference*, Vol. 2, 1205–1208, Bologna, Italy, 1995.